Quantized resonator field coupled to a current-biased Josephson junction in circuit QED

Christian Kraglund Andersen,[1,*] Gregor Oelsner,[2] Evgeni Il'ichev,[2,3] and Klaus Mølmer[1]
[1]*Department of Physics and Astronomy, Aarhus University, DK-8000 Aarhus, Denmark*
[2]*Leibniz Institute of Photonic Technology, P.O. Box 100239, D-07702 Jena, Germany*
[3]*Novosibirsk State Technical University, 20 K. Marx Ave., 630092 Novosibirsk, Russia*
(Received 20 December 2013; published 27 March 2014)

A Lagrangian formalism is used toderive the Hamiltonian for a $\lambda/4$ resonator shunted by a current-biased Josephson junction. The eigenstates and the quantum dynamics of the system are analyzed numerically, and we show that this quantum system can function as an efficient detector of weak incident microwave fields.

DOI: 10.1103/PhysRevA.89.033853 PACS number(s): 42.50.Pq, 03.67.Lx, 85.25.Pb, 85.25.Cp

I. INTRODUCTION

During the last decades, quantum optical system behavior has been implemented in solid-state systems using superconducting Josephson junctions and transmission wave guides [1–4]. In these studies, electric circuit resonators take the place of cavities, while the Josephson junction nonlinearity gives rise to effective few-level systems. The emerging field of circuit quantum electrodynamics (cQED) offers promising perspectives for quantum information processing with manufactured, scalable systems [5–7].

Josephson junctions are used in a vast number of experiments exploring the macroscopic quantum nature of the junction phase variable. This allows studies of macroscopic quantum tunneling and of microwave driving among the quantized levels in the junction [8–11]. The tunneling mechanism of the Josephson junctions is also used as a readout mechanism of metastable qubits in these studies. Josephson junctions are furthermore used in Josephson parametric amplifiers (JPA), where the nonlinearity of the junction allows low-noise amplification of weak microwave fields [12–16]. Today, this technique has led to quantum limited detectors in the microwave regime [17,18], but the detection of single microwave photons is still a major challenge.

Recent works using current-biased Josephson junctions (CBJJ) have made both experimental [19] and theoretical [20–22] progress towards a single microwave photon detector. The aim of this work is to contribute to these developments by studying the response of the CBJJ coupled to a $\lambda/4$ resonator in the few-photon regime (see Fig. 1). The general idea is to use the device both as an amplifier and as a detector, sensitive to a single or a few quanta in the resonator through a classical measurable response in the form of a voltage switch over the Josephson junction.

In Sec. II, we discuss the general framework of cQED and outline the challenges in coupling a junction to a resonator. Section III is devoted to the derivation of the Hamiltonian for the system of a $\lambda/4$ resonator shunted by a CBJJ. We present an eigenvalue analysis of this Hamiltonian in Sec. IV and a time-dependent analysis in Sec. V. Section VI concludes the paper.

*ctc@phys.au.dk

II. COUPLING IN CIRCUIT QED

A microwave transmission waveguide is conveniently described as an infinite series of LC circuits [23]. The coupling of the circuits leads to the identification of oscillator eigenmodes, in which one can quantize the system and obtain the usual Hamiltonian

$$H_T = \sum_j \hbar\omega_j\, a_j^\dagger a_j \tag{1}$$

with ω_j being the angular frequency and a_j ($a_j^\dagger$) being the annihilation (creation) operator of photons in the jth mode. When appropriate (see Sec. III A), a single-mode approximation can be made, which reduces the Hamiltonian to $H_{T,s} = \hbar\omega\, a^\dagger a$.

A CBJJ is described by the effective Hamiltonian [24]

$$H_{JJ} = -\frac{\hbar^2}{2M}\frac{\partial^2}{\partial\varphi^2} - E_J(\cos\varphi + I\varphi), \tag{2}$$

which describes the phase as the position of a particle moving in or trapped in a well of a washboard potential with effective

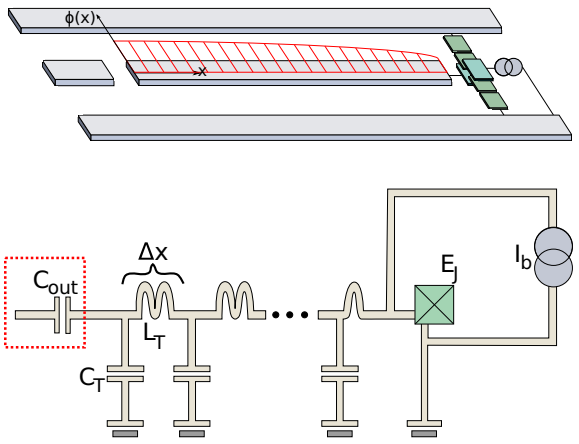

FIG. 1. (Color online) A schematic (top) and a circuit diagram (bottom) of the system. In the upper picture, the fundamental normal mode of the flux is sketched. In the circuit diagram, the transmission waveguide resonator is described as a chain of capacitors and inductors. The resonator is shunted by a current-biased Josephson junction. In the dashed (red) box, we couple capacitively to fields outside of the device.

mass $M = C_J/(2e)^2$, where C_J is the Josephson capacity and E_J is the Josephson energy.

The junction provides an easily accessible readout mechanism as the voltage across the junction will increase when the particle goes from being trapped in a well to running down the potential. Our goal is to provide a consistent theoretical description of the coupling between the motion of the phase particle and the microwave resonator field, i.e., to derive a Hamiltonian in the form

$$H = H_{T,s} + H_{JJ} + H_I, \tag{3}$$

where H_I will contain coupling and interaction terms. Note that we want a full description of the junction degree of freedom. Previous works [2,24–28] on the matter reduce the junction to be either described by a simple two-level system or use the junction in combination with other junctions to create a SQUID, which can also be viewed as a two-level system.

In the well-known Rabi model of a two-level system coupled to a field, the interaction Hamiltonian reduces to $H_I = g(a + a^\dagger)\sigma_x$, where σ_x is the Pauli x matrix. The Rabi model can be solved in the rotating-wave approximation, and also in general [29,30]. However, since we here want to describe the full behavior of the Josephson junction, including the switching dynamics and the dissipation of the junction, we can not in general apply the simple Hamiltonian of the Rabi model.

III. DERIVATION OF THE HAMILTONIAN

In order to obtain the Hamiltonian for the system, we consider the corresponding classical system for which we can directly write up the Lagrangian. With the Lagrangian at hand we can identify the canonical variables and perform a canonical quantization and a Legendre transform to obtain the quantum mechanical Hamiltonian. The approach followed here is similar to the approaches of [23,31–33].

An electrical circuit can be described as a network of electrical elements, e.g., capacitors and inductors, known as branches. We introduce the node variables ϕ_n and q_n associated with every node of the electrical circuit diagram. The flux variable ϕ_n is defined as the time integral of the voltage measured along a path of branches, called the spanning tree, connecting the node to the ground. Branches not included in these paths are called closure branches. The equation of motion for node variables will in general depend on the chosen topology of the spanning tree [23,33].

In Fig. 1, we show a lumped element representation of our system. We will choose the bias line to be a closure branch of the system, while the rest constructs the spanning tree. The resonator is here depicted as a series of n LC circuits, which in the limit $n \to \infty$ will give an appropriate description of the resonator.

This now allows us to write the equation of motion for each node of the resonator, except the end node,

$$C_T \Delta x\, \ddot{\phi}_j = \frac{\phi_{j+1} - \phi_{j-1}}{L_T \Delta x} \quad \text{for} \quad 1 \leqslant j \leqslant n-1, \tag{4}$$

with $\Delta x = d/n$, d being the length of the resonator and C_T and L_T being the capacitance and inductance per length of the resonator. Taking the continuum limit of $\Delta x \to 0$, our sequence of discretized flux variables becomes a function of x, $\phi_j \to \phi(x)$, and Eq. (4) reduces to the wave equation

$$\frac{1}{C_T L_T}\partial_x^2\phi(x) - \partial_t^2\phi(x) = 0. \tag{5}$$

The end point of the circuit is shunted with a bias current I_b, which we model as a high inductance line, with the inductance L_S, pre-charged with a large flux $\tilde{\Phi}_S$, such that $\tilde{\Phi}_S/L_S = I_b$. The equation of motion is then

$$C_J\,\ddot{\phi}_n = \frac{\phi_n - \phi_{n-1}}{L_T \Delta x} - \frac{2e}{\hbar}E_J \sin\frac{2e}{\hbar}\phi_n + \frac{\tilde{\Phi}_S - \phi_n}{L_s}, \tag{6}$$

$$\underset{L_S\to\infty}{=} \frac{\phi_n - \phi_{n-1}}{L_T \Delta x} - \frac{2e}{\hbar}E_J \sin\frac{2e}{\hbar}\phi_n + I_b. \tag{7}$$

We are now able to write the proper Lagrangian for the system, such that the Euler-Lagrange equations give the above equations of motion:

$$\mathcal{L} = \int_0^d dx \left\{ \frac{C_T}{2}[\partial_t\phi(x)]^2 - \frac{1}{2L_T}[\partial_x\phi(x)]^2 \right\} + \frac{C_J[\partial_t\phi(d)]^2}{2} + E_J\left(\cos\frac{2e}{\hbar}\phi(d) + I\,\frac{2e}{\hbar}\phi(d)\right), \tag{8}$$

with $I = I_b/I_c$, where the critical current is defined as $I_c = \frac{2e}{\hbar}E_J$.

The phase across the Josephson junction ϕ_J is given as a function of the bias current

$$\frac{2e}{\hbar}\phi_J = \sin^{-1} I, \tag{9}$$

which will also contribute with a predefined flux in the transmission resonator. If we neglect contributions from the Josephson capacitance C_J, the Euler-Lagrange equation at $x = d$ yields

$$\frac{1}{L_T}\partial_x\phi(d) = \frac{2e}{\hbar}E_j\left(\sin\frac{2e}{\hbar}\phi(d) + I\right). \tag{10}$$

Generally the flux bias will not be constant, but it leads us to the ansatz for solutions of the equation of motion given by

$$\phi(x) = \sum_j \phi_j \cos k_j x + \phi_0. \tag{11}$$

In writing Eq. (11), we have assumed that there is no incident field at the capacitor C_{out}, leading to the open boundary condition $\partial_x\phi = 0$ at $x = 0$. The open boundary condition is equivalent to the assumption of a vanishing current, while the time derivative of $\phi(0)$ yields the voltage at C_{out}, determined by the field inside the resonator. The values of k in Eq. (11) must be chosen to match the boundary condition following from the linearized Euler-Lagrange equation at $x = d$ [Eq. (10)].

Using the steady-state result for the junction phase $\phi_0 = \phi_J$, with the approximation that the phase difference between the phase across the junction and the steady-state phase is small, that is, $\sum \phi_j \cos k_j d \ll 1$, we can derive the following approximate identity:

$$\left(\sin\frac{2e}{\hbar}\phi(d) + I\right) = \frac{2e}{\hbar}\sum_j \phi_j \cos k_j d\, \cos\frac{2e}{\hbar}\phi_0, \tag{12}$$

and we obtain the linearized equation for each independent mode

$$k_j d \tan k_j d = \frac{L_T d}{L_J} \cos \frac{2e}{\hbar}\phi_J, \tag{13}$$

with $L_J = (\hbar/2e)^2/E_J$. This equation can be solved numerically or approximated by

$$k_j d = \frac{\pi(1+2j)}{2\left(1+\frac{L_J}{L_T d \cos\phi_J}\right)}, \tag{14}$$

valid for $L_J \ll L_T d \cos\frac{2e}{\hbar}\phi_J$. We recall that our approximate solutions are only valid when neglecting the Josephson capacitance C_J. In the following, we shall reinstate a contribution from C_J and evaluate its influence on the modes defined in (11).

A. Single-mode approximation

Having Eq. (11) as a solution for the normal modes, we can choose to look at a single-mode field

$$\phi(x) = \phi \cos kx + \phi_0 \tag{15}$$

and substitute this solution into the Lagrangian

$$\begin{aligned}\mathcal{L} = {}& \dot\phi^2\left(\int_0^d \frac{C_T \cos^2 kx}{2}dx + \frac{C_J \cos^2 kd}{2}\right) + \dot\phi_0^2\frac{C_T d + C_J}{2} \\ & + \dot\phi\dot\phi_0\left(\int_0^d C_T \cos kx\, dx + C_J \cos kd\right) \\ & - \phi^2\int_0^d \frac{k^2 \sin^2 kx}{2L_T}dx \\ & + E_J\left(\cos\frac{2e}{\hbar}(\phi\cos kd + \phi_0) + \frac{2e}{\hbar}I(\phi\cos kd + \phi_0)\right).\end{aligned} \tag{16}$$

Next, we expand the cos term of the potential as $\cos(A+B) = \cos A\cos B - \sin A \sin B$ followed by an expansion to fourth order of $(\frac{2e}{\hbar}\phi\cos kd)$ allowing also for Kerr effects in the device. We can reduce the expressions in the Lagrangian significantly by introduction of the quantities

$$C_E = \frac{C_T d}{2}\left(1+\frac{\sin 2kd}{2kd}\right) + C_J\cos^2 kd, \tag{17}$$

$$C_0 = C_T d + C_J, \tag{18}$$

$$C_c = C_T d\,\frac{\sin kd}{kd} + C_J\cos kd, \tag{19}$$

$$L_E^{-1} = \frac{(kd)^2}{2L_T d}\left(1-\frac{\sin 2kd}{2kd}\right). \tag{20}$$

This constitutes the Lagrangian

$$\begin{aligned}\mathcal{L} = {}& \dot\phi^2\frac{C_E}{2} - \phi^2\frac{1}{2L_E} + \dot\phi\dot\phi_0 C_c \\ & + \dot\phi_0^2\frac{C_0}{2} + E_J\left(\cos\frac{2e}{\hbar}\phi_0 + \frac{2e}{\hbar}I\phi_0\right) \\ & - E_J\left(\frac{(2e)^2\phi^2\cos^2 kd}{2\hbar^2} - \frac{(2e)^4\phi^4\cos^4 kd}{24\hbar^4}\right)\cos\frac{2e}{\hbar}\phi_0 \\ & - E_J\frac{2e}{\hbar}\phi\cos kd\left(\sin\frac{2e}{\hbar}(\phi_0-\phi_J)\cos\frac{2e}{\hbar}\phi_J\right. \\ & \left. - \frac{(2e)^2\phi^2\cos^2 kd}{6\hbar^2}\sin\frac{2e}{\hbar}\phi_0\right),\end{aligned} \tag{21}$$

from which we will derive the Hamiltonian. We introduce the conjugate variables to ϕ and ϕ_0,

$$q = \frac{\partial\mathcal{L}}{\partial\dot\phi} = C_E\dot\phi + C_c\dot\phi_0, \tag{22}$$

$$q_0 = \frac{\partial\mathcal{L}}{\partial\dot\phi_0} = C_0\dot\phi_0 + C_c\dot\phi, \tag{23}$$

and we perform a Legendre transformation to get the Hamiltonian

$$\begin{aligned}H = {}& \frac{q_0^2}{2\left(C_0 - C_c^2/C_E\right)} - E_J\left(\cos\frac{2e}{\hbar}\phi_0 + \frac{2e}{\hbar}I\phi_0\right) \\ & - \frac{C_c}{C_0C_E - C_c^2}qq_0 + \frac{q^2}{2\left(C_E - C_c^2/C_0\right)} + \frac{\phi^2}{2L_E} \\ & + E_J\frac{(2e)^2\cos^2 kd}{2\hbar^2}\phi^2\cos\frac{2e}{\hbar}\phi_0 - E_J\frac{(2e)^4\cos^4 kd}{24\hbar^4}\phi^4 \\ & \times\cos\frac{2e}{\hbar}\phi_0 - E_J\frac{2e}{\hbar}\phi\cos kd\left(\sin\frac{2e}{\hbar}(\phi_0-\phi_J)\cos\frac{2e}{\hbar}\phi_J\right. \\ & \left. - \frac{(2e)^2\phi^2\cos^2 kd}{6\hbar^2}\sin\frac{2e}{\hbar}\phi_0\right).\end{aligned} \tag{24}$$

In the quantum regime, the resonator operators q and ϕ satisfy the canonical commutation relation $[\phi,q] = -i\hbar$, which allows us to introduce the ladder operator a ($a^\dagger$) that annihilates (creates) a photon in the normal mode of the resonator. We write

$$\phi = i\sqrt{\frac{\hbar\omega L_E}{2}}(a - a^\dagger), \tag{25}$$

$$q = \sqrt{\frac{\hbar}{2\omega L_E}}(a + a^\dagger) \tag{26}$$

with the angular frequency $\omega = 1/\sqrt{L_E(C_E - C_c^2/C_0)}$.

Now, we introduce the variable $\varphi = \frac{2e}{\hbar}\phi_0$ as well as its conjugate variable q_φ satisfying $[\varphi,q_\varphi] = -i\hbar$. We define $M = (C_0 - C_c^2/C_E)/(2e)^2$ and substitute Eqs. (25) and (26) into the Hamiltonian, while keeping only energy-conserving terms for the cavity field mode and ignoring constant energy shifts and get

$$\begin{aligned}H = {}& \frac{q_\varphi^2}{2M} - E_J(\cos\varphi + I\varphi) + (\hbar\omega + \hbar\eta\cos\varphi)\,a^\dagger a \\ & + \hbar\kappa\cos\varphi\, a^\dagger a^\dagger a a + \hbar\lambda\, q_\varphi q \\ & + (\hbar\mu + \hbar\chi\, a^\dagger a)\,\sin(\varphi - \varphi_J)\,\phi.\end{aligned} \tag{27}$$

This Hamiltonian is the main result of this section. We recognize the Hamiltonian for a single Josephson junction and a single resonator mode coupled by linear and nonlinear terms. The constants in the Hamiltonian are

given as

$$\eta = \frac{E_J}{2}\frac{(2e)^2}{\hbar^2}\cos^2 kd\, L_E\omega, \tag{28}$$

$$\kappa = -\frac{E_J}{4}\frac{(2e)^4}{\hbar^3}\cos^4 kd\, L_E^2\omega^2, \tag{29}$$

$$\lambda = -\frac{2e}{\hbar}\frac{C_c}{C_0C_E - C_c^2}, \tag{30}$$

$$\mu = -\frac{E_J}{\hbar}\frac{2e}{\hbar}\cos kd\, \cos\varphi_J, \tag{31}$$

$$\chi = \frac{E_J}{4\hbar}\frac{(2e)^3}{\hbar^2}\cos^3 kd\, L_E\omega\, \cos\varphi_J. \tag{32}$$

Remembering that $\cos kd$ is assumed to be small, due to the weak field in the resonator, the magnitude of the strengths in frequency units supposedly follow the order $\mu\sqrt{\frac{\hbar\omega L_E}{2}} > \eta > \sqrt{\frac{\hbar\omega L_E}{2}}\chi > \kappa$, while $\lambda\sqrt{\frac{\hbar}{2\omega L_E}}$ does not directly relate to the other quantities. It should also be noted that weak terms which include $\cos\varphi$ but no field coupling terms a or $a^\dagger$ are neglected as they merely change the Josephson energy E_J by a small amount.

B. Validity of the single-mode approximation

The Hamiltonian (27) assumes the near-resonant coupling to only one active resonator mode. The single-mode approximation is valid when the energy difference between modes is much larger than the coupling strengths, but in superconducting circuits, $\mu\sqrt{\frac{\hbar\omega L_E}{2}}$ may be comparable to the mode frequencies, and a more careful analysis is needed.

To illuminate the discussion, we will write the Hamiltonian as

$$H = H_{JJ} + H_{a,JJ} \tag{33}$$

with H_{JJ} equal to the two first terms of Eq. (27) and $H_{a,JJ}$ equal to the rest of the terms involving the fundamental mode a of the resonator. Now, we include a second resonator mode b, and we write the Hamiltonian

$$H = H_{a,JJ} + H_{JJ} + H_{b,JJ} + H_{a,b} \tag{34}$$

with $H_{b,JJ}$ similar to $H_{a,JJ}$ and $H_{a,b}$ representing the direct coupling terms between the two modes caused by the spatially dependent terms in Eq. (8).

We assume that the lowest state of the coupled system is approximately a product state

$$\Psi_0 = \psi_a^0\,\psi_{JJ}^0\,\psi_b^0, \tag{35}$$

while the first excited states for the Hamiltonian in Eq. (34) may be expanded on,

$$\Psi_1 = \psi_{a,JJ}^1\,\psi_b^0 \tag{36}$$

and

$$\tilde{\Psi}_1 = \psi_a^0\,\psi_{b,JJ}^1, \tag{37}$$

where $\psi_{a,JJ}^1$ and $\psi_{b,JJ}^1$ are the first excited eigenstates of $H_{JJ} + H_{a,JJ}$ and $H_{JJ} + H_{b,JJ}$, respectively.

The validity of the single-mode approximation is determined by the coupling of the ground state Ψ_0 and the excited state Ψ_1 to $\tilde{\Psi}_1$:

$$g_{1a,1b} = \int \tilde{\Psi}_1^*(H_{b,JJ} + H_{a,b})\Psi_1, \tag{38}$$

$$g_{0,1b} = \int \tilde{\Psi}_1^*(H_{b,JJ} + H_{a,b})\Psi_0. \tag{39}$$

The system will be driven close to the resonance between Ψ_0 and Ψ_1, and if the conditions

$$|g_{1a,1b}| \ll |\Delta_{1a,1b}|, \quad |g_{0,1b}| \ll |\Delta_{0,1b}| \tag{40}$$

are satisfied, where we have $\Delta_{x,y}$ is the energy difference between states x and y, the coupling can be neglected and the single-mode approximation is justified.

In the calculations in Sec. V we find numerically the conditions in Eq. (40) to be almost satisfied. With parameters used later in the text, we find $|g_{1a,1b}/\Delta_{1a,1b}| \lesssim 0.1$. This will lead to a perturbation of the energy of Ψ_1 by $\sim \hbar\Delta_{0,1a}/100$, and to a population in $\tilde{\Psi}_1$ of 1%. The calculations in Secs. IV and V are performed using the single-mode approximation, and they may hence slightly overestimate the efficiency of the device at the level of 1%. For higher excited states and higher-order resonator modes, we find a decreasing ratio between the coupling strengths and the energy differences, but further theoretical analyses into this matter will be needed to clarify the influence of more modes and levels.

C. Off-resonance and multimode interaction

In the previous section, in order to simplify the problem, we ignored multimode interaction from the term $\dot{\phi}\dot{\phi}_0$, which transforms into coupling of all q_j's. Another way to simplify the problem is to choose the parameters of the resonator such that the energy splittings are much smaller than the energy splittings in the Josephson junction. Then, we safely ignore ϕ_0 as a dynamical variable and replace it with the static value ϕ_J, and from (26) we get $q_j = C_j\phi_j$ with

$$C_j = \frac{C_T d}{2}\left(1 + \frac{\sin 2k_j d}{2k_j d}\right). \tag{41}$$

We can also use the Euler-Lagrange equation (13) and obtain the effective inductance

$$L_j^{-1} = \frac{(k_j d)^2}{2L_T d}\left(1 + \frac{\sin 2k_j d}{2k_j d}\right). \tag{42}$$

Defining $\omega_j = 1/\sqrt{L_jC_j}$ and following the derivation of Eq. (27), we then get the Hamiltonian

$$H = \sum_j(\hbar\omega_j a_j^\dagger a_j + \hbar\kappa_{jj}a_j^\dagger a_j^\dagger a_j a_j) + \sum_{i\neq j}2\hbar\kappa_{ij}a_i^\dagger a_i a_j^\dagger a_j \tag{43}$$

with

$$\kappa_{ij} = -\frac{E_J}{4\hbar}\frac{(2e)^4}{\hbar^2}\cos^2 k_i d\cos^2 k_i d\, L_E^2\omega^2\cos\varphi_J. \tag{44}$$

This Hamiltonian is formally equivalent to the JPA Hamiltonian with κ_{00} being the fundamental JPA Kerr nonlinearity [32]. Unlike the usual setup for a JPA, however, we now

have an easy way of tuning the nonlinearity since $\kappa_{ij} \propto \cos\varphi_J$ can be controlled by the bias current.

IV. SPECTRAL ANALYSIS

After having derived the single-mode Hamiltonian (27), we can choose the realistic parameters [34–36]. We assume a Josephson junction with a zero-coupling critical current $I_c = 2\,\mu$A and a Josephson capacitance $C_J = 1500$ fF together with a 50-Ω-impedance resonator with a bare resonance at 7 GHz. For these parameters, we get $\mu\sqrt{\frac{\hbar L_E \omega}{2}}/\omega \approx 3.5$ for $I = 0.9$, which means that we have ultrastrong coupling between the two systems, hence the rotation-wave approximation breaks down in this regime and we can not approximate the system by a Jaynes-Cummings–type Hamiltonian.

In Fig. 2, we have numerically diagonalized Eq. (27) for parameters chosen as described above. In the diagonalization procedure, the junction phase variable is described on a grid in a box of length 2.5π leaving only one well in the potential of Eq. (2) and the states are now identified as localized wave packets quasibound in the well. We see a bandlike structure given by the number of photons in the resonator and we observe that the higher bands gradually disappear when the bias current is increased. In the end, only the empty cavity with the junction in the ground state survives as a bound state. However, even this state is not bound for $I = 0.94$, which implies that the coupling to the resonator effectively changes the critical current of the junction, as one would expect.

It is also interesting to look at the wave function Ψ for the eigenstates. We expect the resonator field mode and junction phase to be highly correlated due to the ultrastrong coupling terms, however, we can still define the phase distribution

$$P(\varphi) = \int d\phi\, |\Psi(\phi,\varphi)|^2, \tag{45}$$

which we have depicted in Fig. 3 for the first two eigenstates at $I = 0.92$. Since the numerical calculations are done in a Fock basis for the resonator degree of freedom, we use the

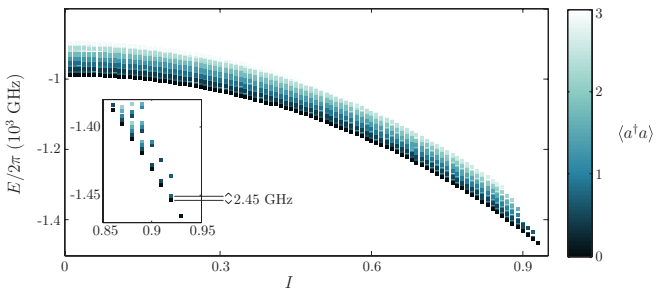

FIG. 2. (Color online) Eigenenergies of the Hamiltonian (27) for different values of the dimensionless bias current I. The color represents the mean value of $a^\dagger a$. The parameters are chosen to represent a Josephson junction with a critical current of 2 μA and a capacitance of 1500 fF. The 50-Ω-impedance resonators bare frequency is chosen to be 7 GHz. Eigensolutions with a mean occupation number in the resonator mode above 3 are not included. In the inset is a zoom of the lowest bands near the end of the bands. Marked with lines in the inset are the eigenenergies in the lowest band at $I = 0.92$, highlighting the energy difference between the only two bound states of the lowest band.

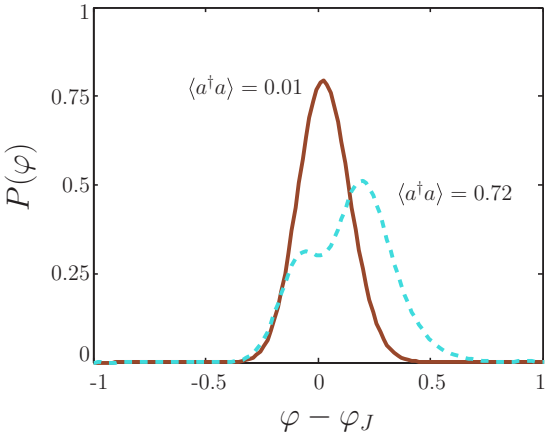

FIG. 3. (Color online) Probability distribution for the Josephson junction phase variable φ calculated with the parameters as in Fig. 2 and $I = 0.92$. This yields the following values for the parameters in Eqs. (28)–(32): $(\eta,\kappa,\lambda\sqrt{\frac{\hbar}{2\omega L_E}},\mu\sqrt{\frac{\hbar\omega L_E}{2}},\chi\sqrt{\frac{\hbar\omega L_E}{2}}) = (5.78, 0.03, 0.90, 29.7, 0.08) \times 2\pi$ GHz. The solid (red) line is the calculated ground state, while the dashed (blue) line is first excited state. The mean value of $a^\dagger a$ for the two states is also indicated in the figure.

partial trace $\langle\varphi|\,\mathrm{Tr}_{\mathrm{res}}(|\Psi\rangle\langle\Psi|)\,|\varphi\rangle$ to calculate the probability distribution. As an interesting feature we see that, even though the ground state is nearly symmetric, the first excited state is very asymmetric. The population in the one-photon state of the resonator effectively lowers the barrier of the potential from Eq. (2) [see also Eq. (55)], which in turn pushes the probability distribution for φ towards the continuum.

A. Coupling of the eigenstates by an external field

We are now interested in driving transitions between the eigenstates of the system. Such a coupling can be realized by coupling the system to the field in an outside resonator through a capacitor with the capacitance C_{out} at $x = 0$ (see dashed box in Fig. 1).

Adding the capacitor gives rise to a Lagrangian term

$$\mathcal{L}_{\mathrm{out}} = \frac{C_{\mathrm{out}}}{2}[\dot\phi_{\mathrm{out}} - \dot\phi(0)]^2, \tag{46}$$

which yields terms quadratic in both $\dot\phi(0)$ and $\dot\phi_{\mathrm{out}}$, but typically C_{out} is much smaller than any other capacitive element so we neglect these terms. In this approximation, the canonical variables are not changed. We can therefore write

$$\dot\phi(0) = \frac{C_0 - C_c}{2\left(C_c^2 - C_E C_0\right)} q + \frac{C_E - C_c}{2\left(C_c^2 - C_E C_0\right)} q_0, \tag{47}$$

$$\dot\phi_{\mathrm{out}} = \sqrt{\frac{\hbar\,\omega_{\mathrm{out}}^2 Z_{\mathrm{out}}}{2}}(b + b^\dagger), \tag{48}$$

with Z_{out} being the impedance of the outside resonator and ω_{out} its frequency. Now, b ($b^\dagger$) annihilates (creates) a photon in the the outside resonator.

In order to estimate the coupling strength of the coupling between the device and the outside field, we look at the spectra

from the Hamiltonian and choose a value of I such that we only have two states in the lowest band. We will now denote these as $|0\rangle$ and $|1\rangle$. From this, we get a term for the Hamiltonian

$$H_{\rm out} = \Omega|0\rangle\langle 1|(b + b^\dagger) + \text{H.c.} \tag{49}$$

with the coupling strength

$$\Omega = \alpha\left(\beta_1\langle 0|q_\varphi|1\rangle + \beta_2\langle 0|a + a^\dagger|1\rangle\right) \tag{50}$$

and the quantities defined by

$$\alpha = C_{\rm out}\sqrt{\frac{\hbar\omega_{\rm out}^2 Z_{\rm out}}{2}}, \tag{51}$$

$$\beta_1 = 2e\frac{C_E - C_c}{2\left(C_c^2 - C_E C_0\right)}, \tag{52}$$

$$\beta_2 = \sqrt{\frac{\hbar}{2L_E\omega}}\frac{C_0 - C_c}{2\left(C_c^2 - C_E C_0\right)}. \tag{53}$$

In writing Eq. (49) we have neglected coupling to higher bands as well as coupling to unbound states, but if we choose $\omega_{\rm out}$ to be resonant with the splitting in the lowest band, this should be a good approximation. Now, if we use the same parameters as before and we set $C_{\rm out} = 5$ fF at a bias current $I = 0.92$ with a frequency of the outside field resonant with the energy splitting $\hbar\omega_{\rm out} = E_1 - E_0$, we get a coupling strength of $|\Omega| = 2\pi \times 29$ MHz. This coupling will also mediate a decay from $|1\rangle$ assuming no external field is applied with a time scale set by the coupling strength.

V. TIME-DEPENDENT ANALYSIS

With a time-independent description in place, we now have to turn to the question of time propagation of the system. If the system is prepared in an eigenstate of the Hamiltonian, the time evolution is at a first glance trivial, however, if the system is prepared with a bias current close to the critical current, there is a finite chance of tunneling through the potential barrier causing a voltage switch across the junction [36–40].

Following the description in Ref. [37], we treat the tunneling loss process by propagating the wave function of the phase variable in a time-dependent imaginary potential (TDIP)

$$i\hbar\frac{\partial\Psi}{\partial t} = [H - iV_{im}(t)]\Psi. \tag{54}$$

The method of [37] also includes a Markovian friction term to take the junction resistance into account. In the simulations we have used a Josephson resistance at 300 Ω.

We use here an ansatz for the TDIP evaluated at each time step as a function of the resonator field mode variable ϕ. Taking the mean of resonator operators in each time step provides an effective potential for the phase particle

$$U_{\rm eff}(\varphi) = \hbar\omega\bar{n} - E_J\left[\cos\varphi\left(1 + \frac{\hbar\eta}{E_J}\bar{n} + \frac{\hbar\kappa}{E_J}\langle a^\dagger a^\dagger aa\rangle\right) + \varphi\left(I + \frac{\hbar\mu}{E_J}\langle\phi\rangle + \frac{\hbar\chi}{E_J}\bar{n}\langle\phi\rangle\right)\right], \tag{55}$$

with $\bar{n} = \langle a^\dagger a\rangle$ being the mean photon number in the resonator field mode at a given time. By taking the mean values we neglect an amount of correlations between the tunneled phase particle and the resonator, however, the tunneling and detection time is much faster than the characteristic time scale of these correlations. With this potential, we can determine the time-dependent classical turning point and, following [37], a useful expression for $V_{im}(\varphi)$.

In the following, we assume that our device is initialized in the ground state and that the resonator is driven with a constant weak classical field, so that

$$(b + b^\dagger)(t) \to \beta\,\sin\omega_{\rm out}t \tag{56}$$

with β a constant of order 1 [41,42]. We thus neglect the operator character of the incident field and the decay from the resonator mode into field modes outside the resonator. Equation (49) then yields

$$H_{\rm out}(t) = \alpha\beta(\beta_1 q_\varphi + \beta_2(a + a^\dagger))\sin\omega_{\rm out}t. \tag{57}$$

In Fig. 4, we present the calculated probability that a switching event has happened, calculated as

$$\mathcal{P}(t) = 1 - ||\Psi(t)||^2 \tag{58}$$

evaluated at the time t and we define the detector efficiency as in [22], $\xi(t) = \mathcal{P}_{\beta=1}(t) - \mathcal{P}_{\beta=0}(t)$. The norm $||\Psi(t)||^2$ is expected to decrease due to the propagation in the TDIP and the tunneling rate can be calculated from the derivative $\gamma = -d||\Psi(t)||^2/dt$. We see that for $\beta = 1$ we approach unit probability within roughly 80 ns, which we may compare with the Rabi time $t_r = \pi/|\Omega| \approx 21$ ns, which implies that around 4 Rabi oscillations are made before a tunneling event is certain. We recall, however, that the Rabi oscillations are modified due to the nonlinear nature of the detector. Nevertheless, the first oscillation can be observed in Fig. 4 as a shoulder on the probability graph around half the Rabi time.

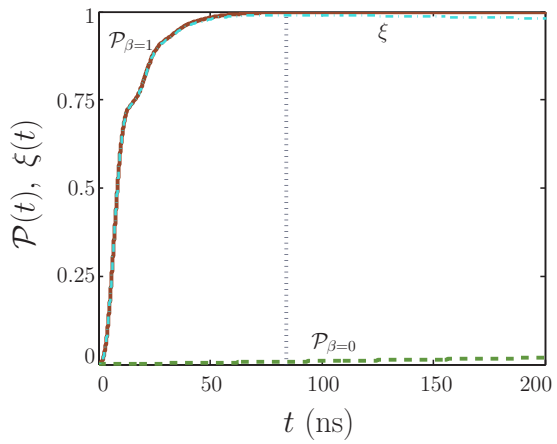

FIG. 4. (Color online) Accumulated probability for a switching event and the detector efficiency for $I = 0.92$. The switching probability for $\beta = 1$ is shown as the solid (red) line, and for $\beta = 0$ as the dashed (green) line. The detector efficiency is shown as the dashed-dotted (blue) line. The dotted vertical line marks the maximal efficiency point. The parameters chosen are those of a Josephson junction with a critical current at 2 μA, a capacitance at 1500 fF, and a Josephson resistance at 300 Ω, thus, Eqs. (28)–(32) yield the same numerical values as in Fig. 3. The 50-Ω-impedance resonator bare frequency is 7 GHz, and we assume $C_{\rm out} = 5$ fF.

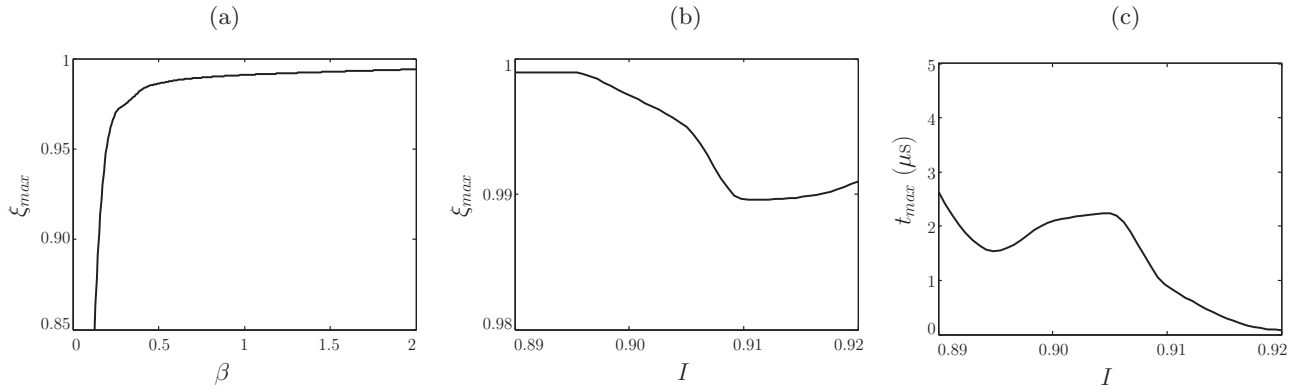

FIG. 5. In (a) we show the maximal detector efficiency for $I = 0.92$ as a function of β, while in (b) the maximal detector efficiency for $\beta = 1$ is shown as a function of I. In (c) we display the detection time required to reach the efficiency in (b). In all figures, ω_{out} is equal to the energy splitting between the two lowest bound states. The rest of the parameters are the same as Fig. 4.

We have also marked the most efficient point in Fig. 4, that is, the maximum of $\xi(t)$. We will denote this efficiency $\xi_{\max}$ and the time where it occurs $t_{\max}$. For the parameters in Fig. 4, we get $\xi_{\max} = 0.991$ with $t_{\max} = 82$ ns. Figure 5 now shows the maximal efficiency as a function of both I and β. In each case, the driving frequency ω_{out} is equal to the energy splitting of the two lowest bound states. This restricts these simulations to $I \leqslant 0.92$, as we do not have more than one bound state above this bias current. As expected, the maximal efficiency increases as the field strength β increases as seen in Fig. 5(a). However, once we are above $\beta = 0.5$, $\xi_{\max}$ saturates. Note that, in our description, a change in β is equivalent to a change in C_{out}. In Fig. 5(b), we see that changing the current to a lower bias current opens for the possibility of even higher quantum efficiency, but in Fig. 5(c) we see that it comes at a price of significantly larger detection time. For the large detection times required for $I < 0.91$, we might not be able to safely neglect decay in the resonator as we have done in these calculations, thus, the efficiency for these values may be smaller than shown in Fig. 5(b). To summarize, we see that our efficiency is close to unity when $\beta > 0.5$ and we get the shortest detection time when $I = 0.92$.

In Fig. 6, we characterize the performance of the detector for a detection time at 82 ns. In Fig. 6(a), we notice that for $I < 0.92$ we quickly lose performance, while at larger I we retain a good detection efficiency. This we can interpret as at lower I we get a suppressed decay rate due to the narrow linewidth of the second lowest energy state in the device, while at larger I we excite directly into the continuum since only one bound state is present. Transferring population directly into the continuum is a weaker process than resonant transfer via an excited bound state, but still stronger than going via a far-detuned narrow state [43–45]. Finally, a slight increase in the efficiency is observed at $I = 0.93$, but here the ground state is very unstable and if the bias current is increased further, no bound state is present in the device.

Figure 6(b) shows that we have a frequency band of around 100 MHz with efficiencies above 0.9, which is substantially larger than the linewidths of state-of-the-art resonators and qubits in cQED [27]. The device thus offers adequate detection efficiency of microwave signals from cQED experiments. We can estimate the relaxation time $T_1 = 1/\Delta\omega$, with $\Delta\omega$ the full width at half maximum of a Lorentzian fit [46]. This yields $T_1 \approx 7.5$ ns, which is a typical order of magnitude for this type of phase qubit [22,46]. It is worth noting that T_1 can be

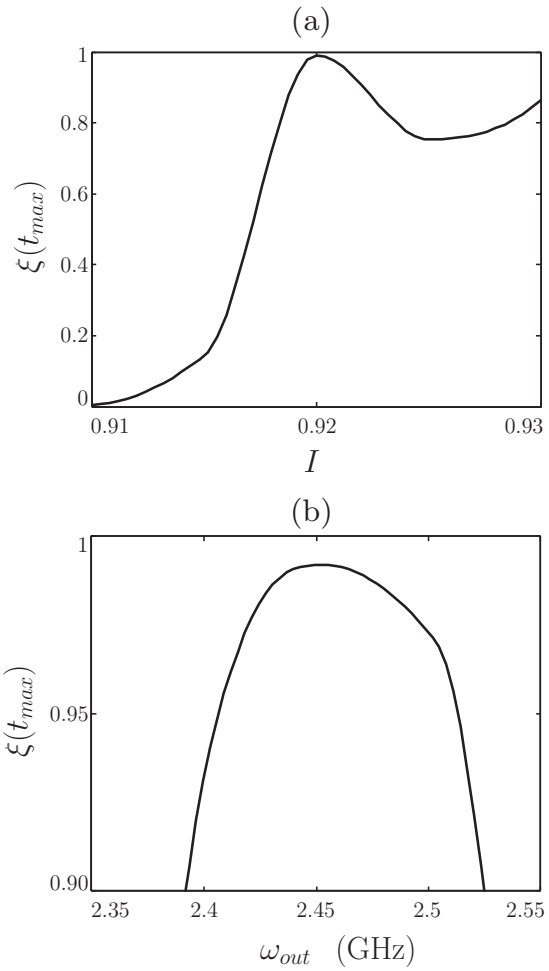

FIG. 6. In (a) we show the detector efficiency as a function of I for fixed $\omega_{\text{out}} = 2.45$ GHz, which is the energy splitting between the two bound states at $I = 0.92$. In (b) the maximal detector efficiency is plotted as a function of ω_{out} for fixed $I = 0.92$. All efficiencies are evaluated at the optimal time $t_{\max} = 84$ ns and other parameters are once again the same as in Fig. 4.

optimized by design of the qubit to improve performance on resonance [22], however, at the expense of a limited bandwidth of the detector. The value of T_1 is smaller than the Rabi time, but this fact does not limit the performance significantly. Coupling the CBJJ directly to the $\lambda/4$ resonator mitigates the limitations imposed by a small T_1 in the setup proposed in [22].

VI. CONCLUSION AND OUTLOOK

In this paper, we have derived the Hamiltonian for a $\lambda/4$ resonator shunted by a current-biased Josephson junction (CBJJ). This device was expected to work as a very sensitive microwave detector near the quantum limit, as it combines the techniques of a JPA to amplify the incoming signal, with the voltage switch of a CBJJ to detect the signal. Numerical calculations show that we indeed get a very high detector efficiency of the device.

Using recently developed theory to describe the switching of a CBJJ [37], the calculations take into account both the complex tunneling dynamics of a CBJJ as well as relaxation in the junction, however, we have neglected losses in the resonator. The method to describe the tunneling uses a time-dependent imaginary potential (TDIP), which is shown in [37] to be a good approximate method. We derive the Hamiltonian using a standard method for quantization of electric circuits [23,33] and we get a coupled resonatorlike degree of freedom and CBJJ-like degree of freedom. This allows us to use the method of [37] to describe the tunneling. We emphasize that we have extended the model of [37] to a junction coupled to a quantized field, but we evaluate the TDIP using mean values of the field. This is an approximation that assumes fast detection of the tunneled phase.

Furthermore, to make sure that resonator losses may be neglected, we seek short optimal detection time, which we get by going to the highest bias current $I = 0.92$, where two bound states still remain in the full system. Here, we get a quantum efficiency at 0.991 at a detection time of 82 ns. Tuning the bias current to a higher value will reduce the efficiency, as bound excited states are lost. Finally, we have shown that at the optimal bias current, within a frequency bandwidth of approximately 100 MHz the efficiency is above 0.9. The calculations have been done based on a single-mode approximation, thus, an experimental implementation might suffer from a small leakage into higher modes of the resonator and thus the efficiency will be slightly reduced or a slightly longer detection time will be required.

The device may be built with current technology, and experimental implementations will provide further insight to the dynamics and performance of the device. Of special interest from a quantum information point of view is the dynamics when the device is coupled to one or more qubits, as the measurement back-action from quantum measurements is known to lead to nontrivial evolution of qubits [47–49]. The measurement back-action on the field degree of freedom of the device is considerably different from the application of the annihilation operator in conventional photon detection [50], and the use of the CBJJ for quantum field detection may thus stimulate development of a novel quantum measurement theory in the microwave domain.

ACKNOWLEDGMENTS

We thank A. C. J. Wade for a careful reading of the manuscript. The authors acknowledge support from the EU 7th Framework Programme collaborative project iQIT.

[1] A. Wallraff, D. Schuster, A. Blais, L. Frunzio, R.-S. Huang, J. Majer, S. Kumar, S. Girvin, and R. Schoelkopf, Nature (London) **431**, 162 (2004).
[2] J. You and F. Nori, Nature (London) **474**, 589 (2011).
[3] Y. Makhlin, G. Schön, and A. Shnirman, Rev. Mod. Phys. **73**, 357 (2001).
[4] D. Vion, A. Aassime, A. Cottet, P. Joyez, H. Pothier, C. Urbina, D. Esteve, and M. H. Devoret, Science **296**, 886 (2002).
[5] A. Blais, J. Gambetta, A. Wallraff, D. I. Schuster, S. M. Girvin, M. H. Devoret, and R. J. Schoelkopf, Phys. Rev. A **75**, 032329 (2007).
[6] V. Zakosarenko, N. Bondarenko, S. Van der Ploeg, A. Izmalkov, S. Linzen, J. Kunert, M. Grajcar, E. Ilichev, and H.-G. Meyer, Appl. Phys. Lett. **90**, 022501 (2007).
[7] L. DiCarlo, J. Chow, J. Gambetta, L. S. Bishop, B. Johnson, D. Schuster, J. Majer, A. Blais, L. Frunzio, S. Girvin *et al.*, Nature (London) **460**, 240 (2009).
[8] J. M. Martinis, M. H. Devoret, and J. Clarke, Phys. Rev. Lett. **55**, 1543 (1985).
[9] J. M. Martinis, M. H. Devoret, and J. Clarke, Phys. Rev. B **35**, 4682 (1987).
[10] J. M. Martinis, S. Nam, J. Aumentado, and C. Urbina, Phys. Rev. Lett. **89**, 117901 (2002).
[11] Y. Yu, S. Y. Han, X. Chu, S. I. Chu, and Z. Wang, Science **296**, 889 (2002).
[12] B. Yurke, L. R. Corruccini, P. G. Kaminsky, L. W. Rupp, A. D. Smith, A. H. Silver, R. W. Simon, and E. A. Whittaker, Phys. Rev. A **39**, 2519 (1989).
[13] T. Yamamoto, K. Inomata, M. Watanabe, K. Matsuba, T. Miyazaki, W. Oliver, Y. Nakamura, and J. Tsai, Appl. Phys. Lett. **93**, 042510 (2008).
[14] M. Castellanos-Beltran, K. Irwin, G. Hilton, L. Vale, and K. Lehnert, Nat. Phys. **4**, 929 (2008).
[15] N. Bergeal, F. Schackert, M. Metcalfe, R. Vijay, V. Manucharyan, L. Frunzio, D. Prober, R. Schoelkopf, S. Girvin, and M. Devoret, Nature (London) **465**, 64 (2010).
[16] C. Eichler, D. Bozyigit, C. Lang, M. Baur, L. Steffen, J. M. Fink, S. Filipp, and A. Wallraff, Phys. Rev. Lett. **107**, 113601 (2011).
[17] A. A. Clerk, M. H. Devoret, S. M. Girvin, F. Marquardt, and R. J. Schoelkopf, Rev. Mod. Phys. **82**, 1155 (2010).
[18] C. Eichler, D. Bozyigit, and A. Wallraff, Phys. Rev. A **86**, 032106 (2012).
[19] Y.-F. Chen, D. Hover, S. Sendelbach, L. Maurer, S. T. Merkel, E. J. Pritchett, F. K. Wilhelm, and R. McDermott, Phys. Rev. Lett. **107**, 217401 (2011).

[20] G. Romero, J. J. García-Ripoll, and E. Solano, Phys. Rev. Lett. **102**, 173602 (2009).
[21] B. Peropadre, G. Romero, G. Johansson, C. M. Wilson, E. Solano, and J. J. García-Ripoll, Phys. Rev. A **84**, 063834 (2011).
[22] A. Poudel, R. McDermott, and M. G. Vavilov, Phys. Rev. B **86**, 174506 (2012).
[23] B. Yurke and J. S. Denker, Phys. Rev. A **29**, 1419 (1984).
[24] M. Devoret, A. Wallraff, and J. Martinis, arXiv:cond-mat/0411174.
[25] Z.-L. Xiang, S. Ashhab, J. Q. You, and F. Nori, Rev. Mod. Phys. **85**, 623 (2013).
[26] A. Omelyanchouk, S. Shevchenko, Y. S. Greenberg, O. Astafiev, and E. Il'ichev, Low Temp. Phys. **36**, 893 (2010).
[27] T. Niemczyk, F. Deppe, H. Huebl, E. Menzel, F. Hocke, M. Schwarz, J. J. García-Ripoll, D. Zueco, T. Hümmer, E. Solano *et al*., Nat. Phys. **6**, 772 (2010).
[28] J. Bourassa, J. M. Gambetta, A. A. Abdumalikov, O. Astafiev, Y. Nakamura, and A. Blais, Phys. Rev. A **80**, 032109 (2009).
[29] D. Braak, Phys. Rev. Lett. **107**, 100401 (2011).
[30] L. Yu, S. Zhu, Q. Liang, G. Chen, and S. Jia, Phys. Rev. A **86**, 015803 (2012).
[31] M. Wallquist, V. S. Shumeiko, and G. Wendin, Phys. Rev. B **74**, 224506 (2006).
[32] C. Eichler and A. Wallraff, EPJ Quantum Technology **1**, 2 (2014).
[33] M. H. Devoret, in *Proceedings of Les Houches Summer School, Session LXIII, 1995*, edited by S. Reynard, E. Giacobino, and J. Zinn-Justin (Elsevier, Amsterdam, 1997).
[34] P. Macha, S. van Der Ploeg, G. Oelsner, E. Ilichev, H.-G. Meyer, S. Wunsch, and M. Siegel, Appl. Phys. Lett. **96**, 062503 (2010).
[35] G. Oelsner, L. Revin, E. Il'ichev, A. Pankratov, H.-G. Meyer, L. Gronberg, J. Hassel, and L. Kuzmin, Appl. Phys. Lett. **103**, 142605 (2013).
[36] H. F. Yu, X. B. Zhu, Z. H. Peng, W. H. Cao, D. J. Cui, Y. Tian, G. H. Chen, D. N. Zheng, X. N. Jing, L. Lu, S. P. Zhao, and S. Han, Phys. Rev. B **81**, 144518 (2010).
[37] C. K. Andersen and K. Mølmer, Phys. Rev. A **87**, 052119 (2013).
[38] G. S. Paraoanu, Phys. Rev. B **72**, 134528 (2005).
[39] M. V. Fistul, A. Wallraff, and A. V. Ustinov, Phys. Rev. B **68**, 060504 (2003).
[40] Sun Guozhu, Wang Yiwen, Cao Junyu, Chen Jian, Ji Zhengming, Kang Lin, Xu Weiwei, Yu Yang, Han Siyuan, and Wu Peiheng, Phys. Rev. B **77**, 104531 (2008).
[41] A. E. B. Nielsen and K. Mølmer, Phys. Rev. A **77**, 052111 (2008).
[42] H. Carmichael, *Statistical Methods in Quantum Optics 2: Non-Classical Fields*, Vol. 2 (Springer, Berlin, 2008).
[43] S. Guérin and H.-R. Jauslin, Phys. Rev. A **55**, 1262 (1997).
[44] W. Cai, T. F. Zheng, P. Hu, M. Lax, K. Shum, and R. R. Alfano, Phys. Rev. Lett. **65**, 104 (1990).
[45] F. Grossmann, T. Dittrich, P. Jung, and P. Hänggi, Phys. Rev. Lett. **67**, 516 (1991).
[46] A. J. Berkley, H. Xu, M. A. Gubrud, R. C. Ramos, J. R. Anderson, C. J. Lobb, and F. C. Wellstood, Phys. Rev. B **68**, 060502 (2003).
[47] K. Murch, S. Weber, C. Macklin, and I. Siddiqi, Nature (London) **502**, 211 (2013).
[48] J. E. Johnson, C. Macklin, D. H. Slichter, R. Vijay, E. B. Weingarten, J. Clarke, and I. Siddiqi, Phys. Rev. Lett. **109**, 050506 (2012).
[49] D. Ristè, J. G. van Leeuwen, H.-S. Ku, K. W. Lehnert, and L. DiCarlo, Phys. Rev. Lett. **109**, 050507 (2012).
[50] R. J. Glauber, Phys. Rev. **130**, 2529 (1963).